16. K. Kinoshita and P. Stonehart, *Electrochim. Acta,* **23**, 45 (1978).
17. J. B. Goodenough, A. Hamnett, B. J. Kennedy, and S. A. Weeks, *ibid.,* **32**, 1233 (1987).
18. L. P. Hillenbrand and J. W. Lacksonen, *This Journal,* **112**, 245 (1965).
19. B. Bittins-Carraneo and T. Iwasita, *J. Electroanal. Chem.,* **238**, 151 (1987).
20. S. J. Tauster, S. L. Fung, and R. T. Garten, *J. Am. Chem.*

Soc., **100**, 170 (1978).
21. A. K. Shukla, K. V. Ramesh, R. Manoharan, P. R. Sarode, and S. Vasudevan, *Ber. Brunsenges. Phys. Chem.,* **89**, 1261 (1985).
22. K. S. Kim, N. Winograd, and R. E. Davis, *J. Am. Chem. Soc.,* **93**, 6296 (1971).
23. G. C. Allen and P. M. Tucker, *J. Electroanal. Chem.,* **50**, 335 (1974).
24. B. J. Kennedy and A. Hamnett, *ibid.,* **283**, 271 (1990).

Electron-Transfer Reactions on Passive Chromium

Thomas P. Moffat,*[,a] Hongjun Yang,[b] Fu-Ren F. Fan, and Allen J. Bard*

Department of Chemistry, University of Texas, Austin, Texas 78712

ABSTRACT

The kinetics of electron transfer between electrochemically passivated chromium and several outer-sphere redox couples have been investigated as a function of passive-film thickness, $d = 5$ to 25 Å, in $1M$ H_2SO_4. The apparent rate of electron transfer decreased exponentially with increasing thickness of the passivating overlayer. Similarly, during potentiostatic film growth, the electron-transfer rate decreased logarithmically with time, t, as a consequence of the film-growth kinetics, since d varies with $\log(t)$. These relationships indicate an electron-tunneling controlled process. However, variations in the film thickness and defects result in electron transfer occurring at distributed sites of enhanced tunneling probability, making a meaningful quantitative analysis difficult.

Chromium plays an essential role in the corrosion resistance of many engineering alloys. Protection results from the formation of a thin, ~5-25 Å, passivating oxide film. The electrochemical characteristics of this electrode are determined by reactions involving both ions and electrons. The passive film blocks ion-transfer processes associated with metal dissolution. The kinetics of film formation indicate that ion transport across the protective film occurs by a high field mechanism.[1,2] To sustain the high field condition, the film must be electronically insulating. In contrast, the reversible potential and associated redox kinetics of the $Fe^{3+}_{(aq)}/Fe^{2+}_{(aq)}$ electron-transfer reaction have been readily measured on a passive chromium electrode.[3] The relatively facile nature of this reaction leads to the contradictory suggestion that the passive film is electronically conducting.[3,4] Theoretical studies address this question of film conductivity by invoking electron tunneling through the thin depleted semiconducting oxide film.[5,6] Chromium with its native oxide has been used previously to construct solid-state tunneling junctions.[7] Similarly, the tunneling process has been used with varying degrees of rigor, to describe redox reactions occurring on oxidized tin,[8] iron,[9] nickel,[9] chromium,[9] stainless steel,[9] and SnO_2.[10] However, no detailed electron-transfer studies have been performed on electrochemically passivated chromium.

Much effort has been expended to resolve the influence of tunneling in heterogeneous electron-transfer reactions. Many of these studies have been hampered by complications arising from the probing redox couple (*e.g.,* O_2/H_2O on Pt^{11}) or ambiguities associated with the tunneling barrier (*e.g.,* pinhole defects in alkylthiol barriers on gold).[12] The influence of the tunneling process should be most evident for films ranging from 5 to 30 Å in thickness.[5,6] This corresponds precisely to the thickness range of the passivating film found on chromium. The rate of charge transfer across this barrier should reflect the electronic properties of the film as well as its thickness. Here we describe the kinetics of electron transfer between several simple outer-sphere redox couples and a chromium electrode as a function of passive film thickness.

Overview of the electrochemistry of chromium.—Combined surface analytical and electrochemical studies have

generated significant information concerning the passive state of chromium.[1,2] The characteristic i-E curve for chromium in sulfuric acid is given in Fig. 1. The active-passive transition, associated with a five-orders-of-magnitude decrease in reactivity, is apparent at ~ -0.439 V. Active dissolution yields chromous ions, while passivation is associated with the formation of the blocking passive layer. A small cathodic current loop, due to proton reduction on the
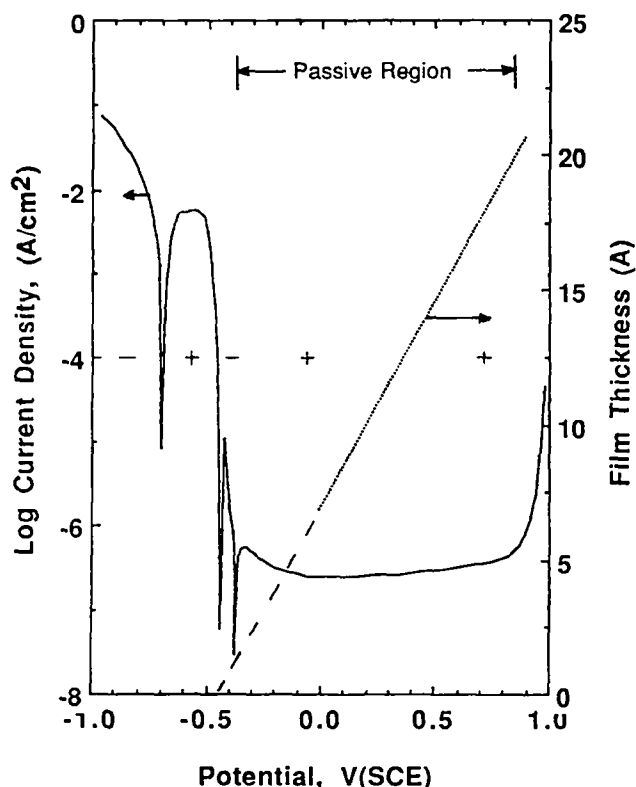
Fig. 1. The i-E polarization curve of chromium in deaerated $1M$ H_2SO_4 for a sweep rate of 0.1 mV/s. The plus and minus signs denote regions of net anodic and cathodic current, respectively. The potential dependence of the passive film thickness is indicated. These data were derived from XPS measurements of electrodes following 1 h of potentiostatic polarization.[2]

* Electrochemical Society Active Member.
a Present address: NIST, 224/B166, Gaithersburg, Maryland 20899.
b Present address: IGEN, Inc., Rockville, Maryland 20852.

passive surface is observed in the region of -0.40 V. The anodic current in the passive regime is almost independent of potential. X-ray[1,2] and optical[13,14] spectroscopic studies indicate that the passive film is a hydrated chromic oxy-hydroxide, $CrOOH-(H_2O)_x$. The thickness of the film is a linear function of potential ($\sim$15.5 Å/V), while the electrode capacitance is inversely proportional to potential. Therefore, in congruence with high-field growth kinetics, the passive overlayer may be described as a simple dielectric with $\varepsilon \sim 25$. The film is stable against reduction, as long as the potential is not swept into the active regime (*i.e.*, more negative than -0.45 V). At more positive potentials (>0.8 V), transpassive dissolution occurs with the production of soluble chromate. The onset of this reaction also is associated with the generation of higher valent species in the film as revealed by voltammetric measurements.[2]
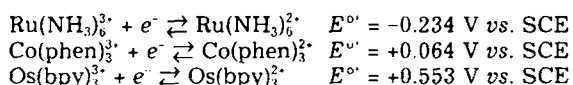
Experimental Procedure

High-purity chromium was provided by F. A. Schmidt of Ames Laboratory, Ames, Iowa. Mass spectroscopic analysis revealed that the arc-melted specimen contained 48 ppm oxygen and was 99.988% pure with respect to metals. The average grain diameter was 0.4 cm. For electrochemical measurements, a standard three-electrode cell was used in conjunction with a PAR 173/376 potentiostat, Norland 3001/MAX oscilloscope, and an X-Y recorder. The electrolyte was $1M$ H_2SO_4 which was deaerated with argon and maintained at 30°C unless otherwise noted. A saturated mercurous sulfate reference electrode (MSE) was used for performing the experiments, although all potentials reported in this paper are referred to the more common saturated calomel electrode (SCE)

$$E(SCE) = E(MSE) + 0.444 \text{ V in } 1M \text{ } H_2SO_4$$

Passive film growth.—The thickness of the passive film (*d*) is a linear function of potential and logarithmically dependent on time.[1,2,14] As with most thin-film solids, the detailed properties of the passive layer are a strict function of the formation conditions; consequently, a direct comparison between data sets requires careful specification of these parameters. The following film-growth program was used. Initially the electrode was activated in the test solution at -0.8 V for at least 15 s. The potential then was stepped to the film-growth potential of interest, and after 1 h, the electron-transfer experiments were performed. The potential was increased by 100 mV increments (without reactivating) to grow thicker films for successive experiments. In complementary work, the electron-transfer kinetics were measured as a function of time and temperature for a given potential.

Electron-transfer kinetics.—The kinetics of three different outer-sphere redox couples were examined on passivated chromium

$Ru(NH_3)_6^{3+} + e^- \rightleftarrows Ru(NH_3)_6^{2+}$ $E^{0'} = -0.234$ V *vs.* SCE
$Co(phen)_3^{3+} + e^- \rightleftarrows Co(phen)_3^{2+}$ $E^{0'} = +0.064$ V *vs.* SCE
$Os(bpy)_3^{3+} + e^- \rightleftarrows Os(bpy)_3^{2+}$ $E^{0'} = +0.553$ V *vs.* SCE

where phen represents 1, 10-phenanthroline; bpy, 2,2'-bipyridine. These reactions exhibit well-defined voltammetric behavior on gold. Consequently, gold ultramicroelectrodes were used to measure the intrinsic rate of these systems using cyclic voltammetry. The heterogeneous kinetics of these reactions are defined by the formal potential, $E^{0'}$, standard rate constant, k^0, and transfer coefficient, α. The k^0 for $Ru(NH_3)_6^{3+/2+}$, evaluated with a 50 µm diameter ultramicroelectrode, was 0.85-5.5 cm/s. Table I lists the experimentally observed peak splitting (ΔE_p) values for a variety of sweep rates. These measurements were sensitive to the electrode pretreatment. However, reasonably precise results were obtained if the specified cleaning step was performed prior to each measurement. Voltammetry performed at high sweep rates is systematically distorted by solution resistance and electrode capacitance. Therefore, the upper limit of the rate constant for $Ru(NH_3)_6^{3+/2+}$ corresponded to the sweep rate at which devia-

Table I. Voltammetric data for 1 mM $Ru(NH_3)_6^{3+}$ reduction at a 50 µm diameter Au microelectrode in $1M$ H_2SO_4.

v (V/s)	ΔE^{*}_p (mV)	k^0_{eff} (cm/s)
1000	90	0.85
800	86	0.94
600	74	1.4
500	70	1.8
400	67	2.4
300	59	>5.5

Reproducibility of ΔE_p data for Au electrode.

Electrode preparation	ΔE_p (v = 1000 V/s)
Clean electrode by cycling potential between 1.444 and -0.666 V *vs.* SCE before collecting each voltammogram. (0.073 to -0.471 V *vs.* SCE)	78
	86
	94
	86
	90
	94
	98
	94
	90
	86
	90 Avg

tion from reversible behavior was first noted, *i.e.*, 400 V/s. The k^0 values listed in Table I agree favorably with those derived from Tafel plot measurements on various metal electrodes, *e.g.*, Au, Ag, Pt, Pd, Cu, and Hg, under turbulent pipe-flow conditions (0.5-1.2 cm/s).[15] The cathodic and anodic transfer coefficients were 0.51 ± 0.05 and 0.41 ± 0.04, respectively.[15] The diffusion coefficient, *D*, of $Ru(NH_3)_6^{3+}$, determined from the steady-state diffusion-limited current at 50 and 100 µm diameter ultramicroelectrodes, was 1.18 × 10^{-5} cm^2/s at 30°C. The temperature dependence of the diffusion coefficient was evaluated by examining the peak current of the reversible voltammograms, between 0°C and 30°C, yielding (with *T* in K)

$$D(T) = 5.5 \times 10^{-5} - 1.3 \times 10^{-2} \left(\frac{1}{T}\right) \qquad [1]$$

Similarly, k^0 for $[Os(bpy)_3]^{3+/2+}$, at 30°C, was 0.38-3.2 cm/s, while that for $[Co(phen)_3]^{3+/2+}$ was 0.066 cm/s.

In a similar fashion, the rate of electron transfer on passivated chromium, with varying film thickness, was characterized by an effective standard rate constant, k^0_{eff}, and transfer coefficient α_{eff}. These parameters were measured by cyclic voltammetry or steady-state log *i* *vs.* *E* (Tafel) analysis.[16]

Cyclic voltammetry.—The kinetics of $Ru(NH_3)_6^{3+/2+}$ and $Os(bpy)_3^{3+/2+}$ on gold and passive chromium were measured by voltammetry performed over a range of potential sweep rates, v, of 0.005-1000 V/s. The effective rate constant and transfer coefficient were evaluated by comparing the data with digital simulations based on the well-developed theory of quasi-reversible one-electron-transfer reactions.[16] To expedite this process, theoretical working curves were constructed based on four experimental parameters; $\Delta E_p = E_{pc} - E_{pa}$, $E_{pc} - E^{0'}$, $E_{pc} - E_{pc/2}$, and $\Psi(E)$, *vs.* the logarithm of the dimensionless parameter Λ, where E_{pc} and E_{pa} are the cathodic and anodic peak potentials, $E_{pc/2}$ is the half-peak potential, $\Psi(E)$ is the current function, defined as

$$\Psi(E) = \frac{i}{nFAC_oD^{1/2}\left(\frac{nF}{RT}\right)^{1/2}v^{1/2}} \qquad [2]$$

and Λ is the dimensionless rate parameter

$$\Lambda = \frac{k^0}{D^{1/2}\left(\frac{nF}{RT}\right)^{1/2}v^{1/2}} \qquad [3]$$

where *n* is the number of equivalents, *A* is the geometrical electrode area, and C_o is the bulk concentration. This was
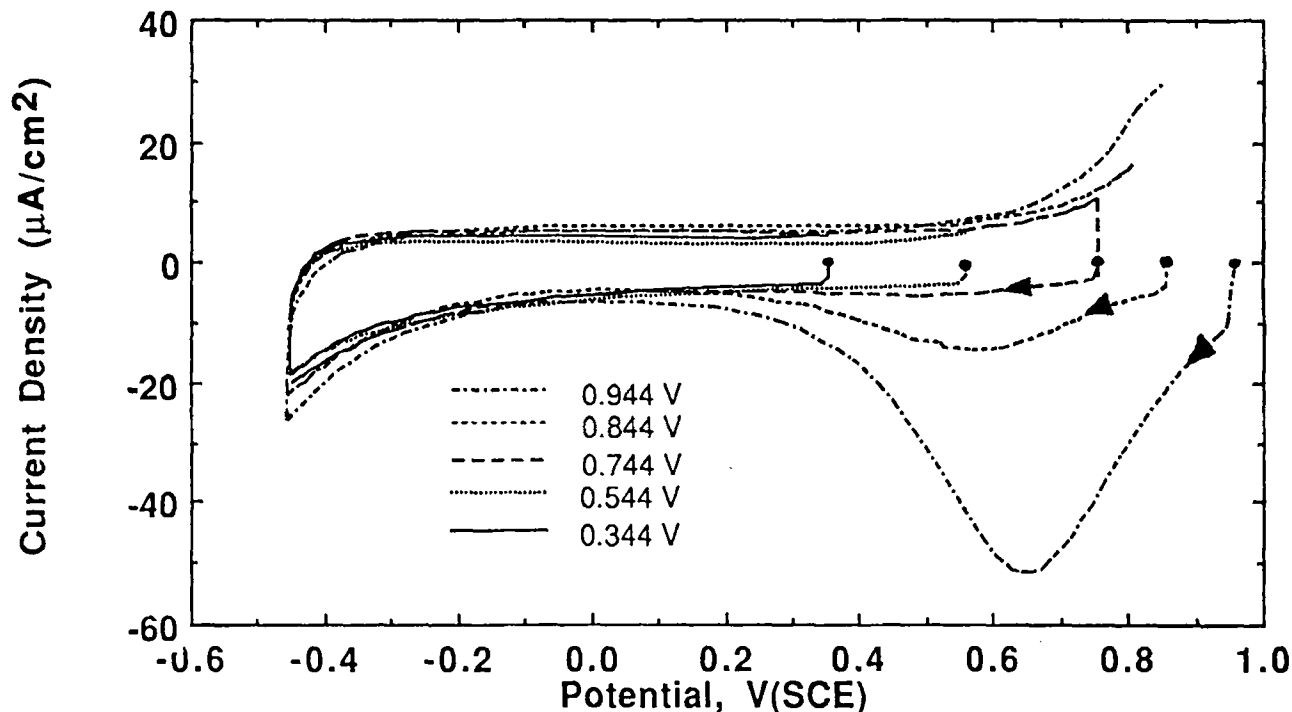
Fig. 2. Voltammograms for passive films grown for 1 h at the potential indicated by the solid circle; v = 0.1 V/s in argon deaerated 1M H₂SO₄.

done in increments of 0.05 for the transfer coefficient. Values of k_{eff}^o and α_{eff} were evaluated by graphically iterating between these figures until a suitable match was found. In some cases, these rate parameters were used to generate complete voltammetric curves. The background charging currents were not explicitly treated in this analysis.

Tafel analysis.—For $[\text{Co(phen)}_3]^{3+/2+}$ the rate of electron transfer on passive chromium was much lower than on gold. In this instance k_{eff}^o and α_{eff} were obtained easily from a Tafel plot, $\log(i)$ *vs.* E, assuming that the concentration of redox species near the electrode was unperturbed over the potential range investigated. The best-fit linear slope of the curve gives α_{eff}

$$\frac{\partial E}{\partial \log(i)} = -2.303 \frac{RT}{\alpha_{\text{eff}} F} \qquad [4]$$

while the intercept with the formal potential yields i_o, the exchange current, and k_{eff}^o (cm/s)

$$k_{\text{eff}}^o = \frac{i_o}{n F C_o A} \qquad [5]$$

Results

Passive chromium.—The redox behavior of the as-grown passive film on chromium was investigated by voltammetry. For films grown at potentials less than 0.544 V, the voltammogram essentially represents the capacitive discharging and charging of the CrOOH · (H₂O)$_x$ dielectric film (Fig. 2). At higher potentials, $E > 0.550$ V, the film undergoes further oxidation as shown by a reduction peak on the "negative going" scan. Capacitance and chronoamperometric measurements are consistent with a change in film composition occurring at these potentials.[1,2] The transformation may be assigned to either the conversion of Cr^{3+} to Cr^{4+} by electron-proton injection/ejection and/or to the formation of a Cr^{3+}/Cr^{6+} mixed valent oxide.[1,2]

Ru(NH₃)₆³⁺/²⁺.—A typical capacitive voltammogram for chromium passivated at 0.444 V is shown in Fig. 3(b). When the same experiment is performed in a solution containing 1 mM Ru(NH₃)₆Cl₃, reduction and oxidation waves for the redox couple appear (Fig. 3(a)). A simulation for a simple quasi-reversible one-electron-transfer reaction (curve c) agrees favorably with the data (curve a). Similar results were obtained for films grown at other potentials. The ap-

parent rate constants, k_{eff}^o, were extracted from the voltammograms (Fig. 4). The best fit between experiment and theory was for a transfer coefficient of 0.50 ± 0.05. The effective rate constant, k_{eff}^o, decreased exponentially with an increase in the potential of film formation. The k_{eff}^o values plotted represent the average obtained from experiments performed at several different scan rates. The whole experiment was repeated four times, and the k_{eff}^o values were reproducible to the extent indicated by the error bars in Fig. 4.

Os(bpy)₃³⁺/²⁺.—The same experiments were performed with 1 mM Os(bpy)₃(ClO₄)₂ as the probing redox species. In this instance peak splitting, ΔE_p, alone was used to estimate k_{eff}^o. The derived rate constant was identical to that measured for Ru(NH₃)₆³⁺/²⁺ under similar conditions. As shown in Fig. 4, the rate decreased exponentially with increasing film-formation potential. However, k_{eff}^o values for this couple, with a more positive $E^{o'}$, are not as precise as those for Ru(NH₃)₆³⁺/²⁺. The measurement of k_{eff}^o for films grown below the formal potential of Os(bpy)₃³⁺/²⁺ required that the potential be swept in the positive direction where additional film growth may occur. Moreover, the rate constants derived for films grown above the formal potential are complicated by the oxidation of the redox couple during film growth. This perturbs the boundary conditions utilized in the analysis of the voltammetric data. Finally, at potentials greater than 0.55 V the passive film itself exhibits some redox activity. Thus, the rate constants measured in this regime are probing a mixed-valent oxide, while in the case of the Ru(NH₃)₆³⁺/²⁺ data this mixed valency is removed prior to the electron transfer measurement.

Co(phen)₃³⁺/²⁺.—The slower kinetics of the Co(phen)₃³⁺/²⁺ couple facilitates the simple application of Tafel analysis. The $\log(i)$-E plots for films formed at various potentials in a 1 mM Co(phen)₃(ClO₄)₃ solution are given in Fig. 5. These data also reveal the redox activity of the passive films formed above +0.55 V. The effective rate constant and transfer coefficient obtained from the Tafel plots are summarized in Fig. 4 and 6. In agreement with the results for the other redox couples, the rate of electron transfer decreased exponentially with increasing film-formation potential. Simultaneously, the apparent cathodic transfer coefficient decreased monotonically from 0.5 This deviation may result from measuring the slope at different over-
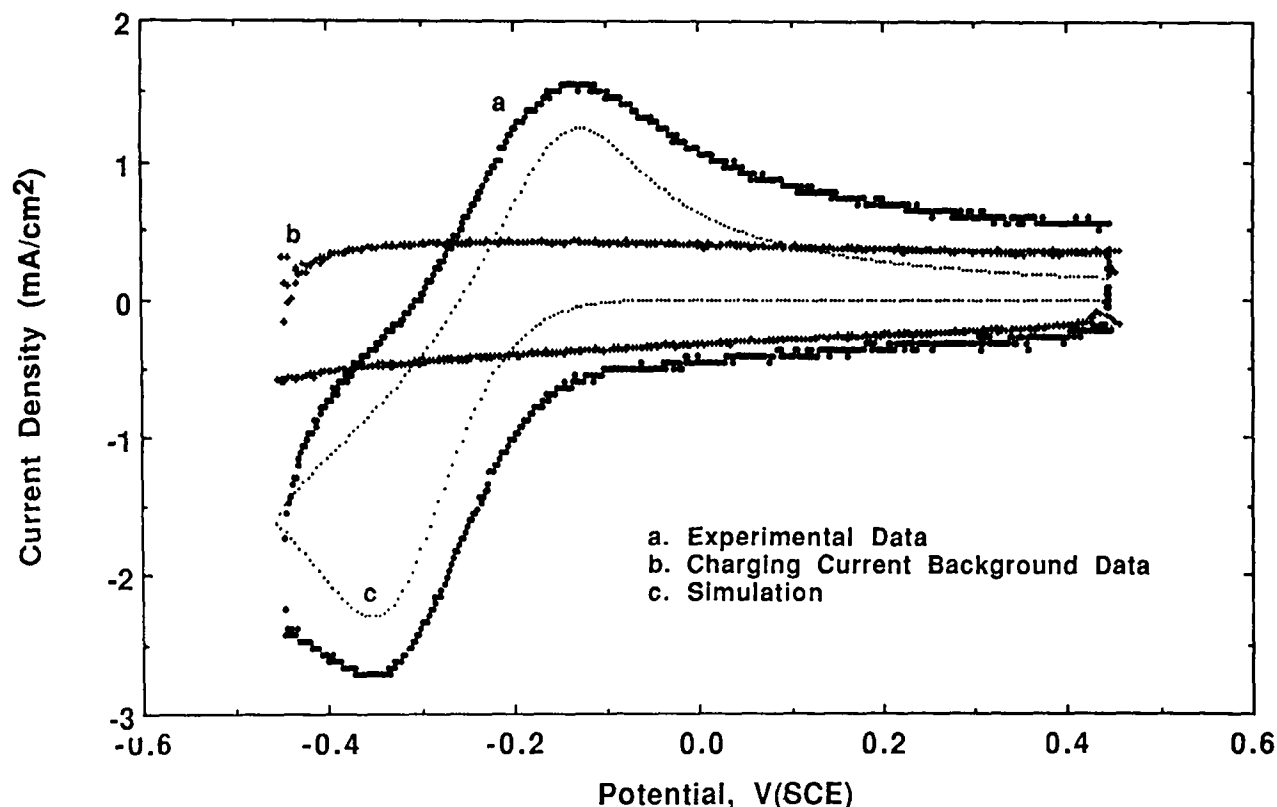
Fig. 3. Voltammetry of (a) 1 m*M* Ru(NH₃)₆³⁺ and (b) the background charging current for chromium passivated at 0.444 V, in deaerated 1*M* H₂SO₄, ν = 10 V/s. (c) Simulation for a simple quasi-reversible one-electron-transfer reaction, in the absence of changing current with k_{eff}^o = 0.01 cm/s, α = 0.5.
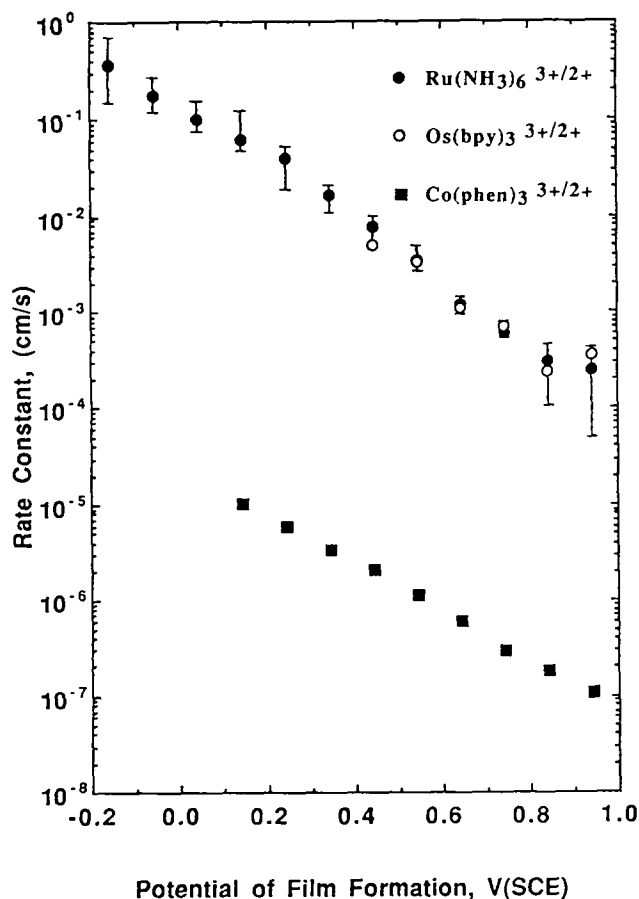
Fig. 4. The apparent rate constant as a function of the film-growth potential. The error bars pertain to variations of the rate constant for Ru(NH₃)₆³⁺/²⁺, determined from four independent experiments.

potentials, *i.e.*, sampling of Tafel plot curvature as predicted by Marcus theory.[6] In this case the apparent rate constant will be artificially high.

Dependence of k_{eff}^o on film thickness.—As noted in Fig. 1, the thickness of the passive film is a monotonic function of the potential of film formation. The thickness data were obtained from a recently published x-ray photoemission (XPS) study.[2] While a degree of uncertainty surrounds the precise value of film thickness used in this study, the favorable comparison between the XPS data[1,2] and prior ellipsometry data[14] is encouraging. Consequently, the kinetics of electron transfer can be correlated to the passive-film thickness (Fig. 7). This reveals that the electron-transfer rate is exponentially dependent on film thickness, d

$$k_{eff}^o = \mathscr{A} \exp(-\beta d) \qquad [6]$$

with β ranging from 0.215 Å⁻¹ for Ru(NH₃)₆³⁺/²⁺ and Os(bpy)₃³⁺/²⁺ to 0.164 Å⁻¹ for Co(phen)₃³⁺/²⁻. For the Ru(NH₃)₆³⁺/²⁺ data, extrapolation of the curve to zero film thickness yields an intrinsic rate constant near that observed on the gold electrode. A similar relationship holds for the Os(bpy)₃³⁺/²⁺ data, which indicates the dominating influence of film thickness as opposed to differences in the relative energetics of the respective redox couples. The Co(phen)₃³⁺/²⁺ rate data exhibit a similar dependence on film thickness; however, extrapolation to zero thickness gives a rate constant two orders of magnitude below the value measured for gold. This discrepancy might arise from the differing measurement schemes employed. Specifically, the concept of active area is at issue. In the Tafel analysis (Co(phen)₃³⁺/²⁺: Cr) the rate constant is explicitly dependent on the electrochemically active area while peak splitting, ΔE_p, which was used predominantly in the analysis of the voltammetric data (Ru(NH₃)₆³⁺/²⁺, Os(bpy)₃³⁺/²⁺: Cr, Au and Co(phen)₃³⁺/²⁺: Au) is not a function of the active area.

Rate constant measured during film growth.—The relationship between the kinetics of electron transfer and film
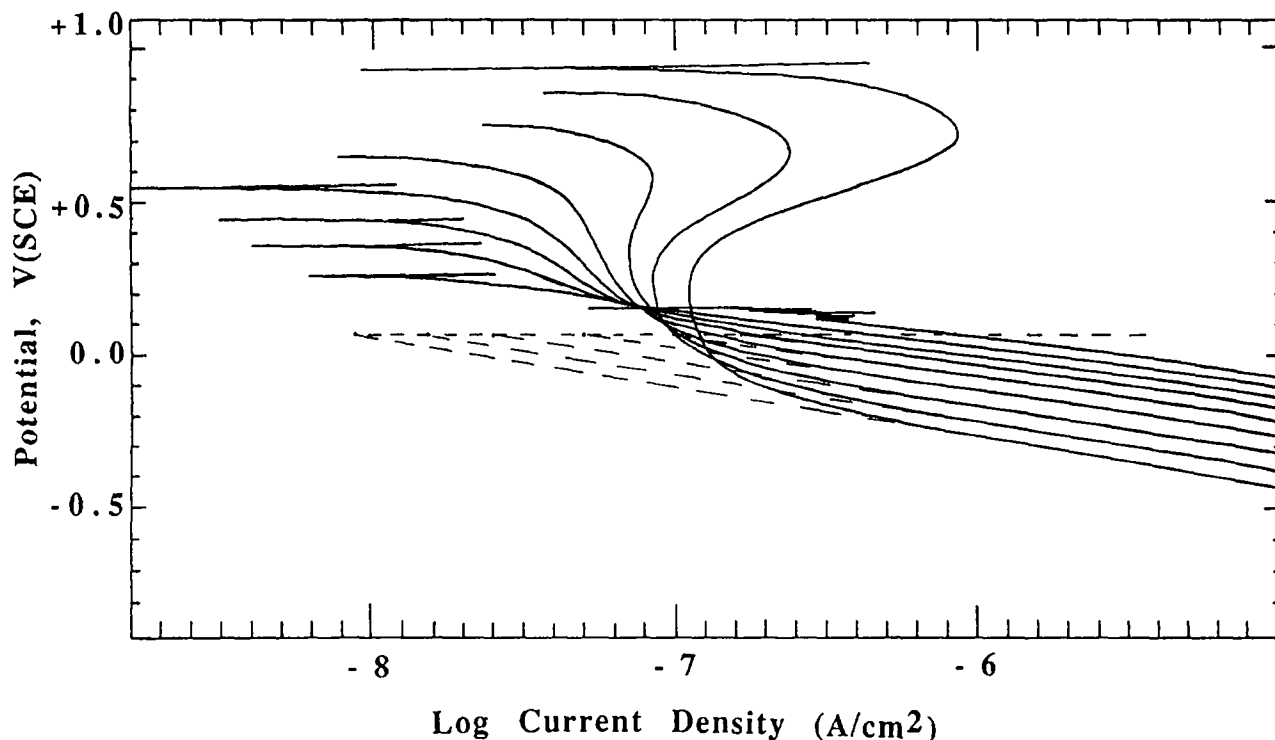
Fig. 5. Tafel plots for the reduction of Co(phen)$_3^{3+}$ at a sweep rate of 2 mV/s. The dotted lines represent the best-fit Tafel slope extrapolated to the formal potential of Co(phen)$_3^{3+/2+}$. In agreement with Fig. 2, the onset of Cr^{3+} oxidation within the passive film becomes apparent for films grown above 0.55 V. However, as with the Ru(NH$_3$)$_6^{3+/2+}$ experiments, the mixed valency was removed prior to the reduction of Co(phen)$_3^{3+}$.

thickness also can be demonstrated by monitoring the redox kinetics during film growth. At a given potential, passive film growth occurs as a logarithmic function of time,[1]
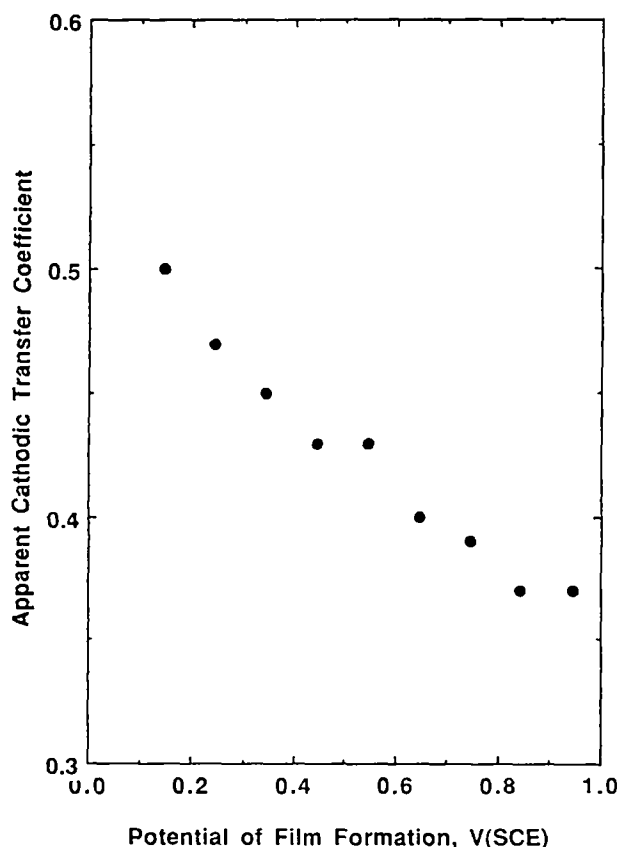
Fig. 6. The apparent cathodic transfer coefficient for Co(phen)$_3^{3+}$ reduction on passive chromium. The coefficient was obtained from the slope of the dotted-lines shown in Fig. 5.

i.e., $d \propto \log(t)$. Electron-transfer kinetics were measured by interrupting potentiostatic film growth with cyclic voltammograms probing Ru(NH$_3$)$_6^{3+/2+}$ reduction and oxidation. In these experiments, a freshly polished electrode was prepared by first activating at –0.8 V followed by passivation at –0.156 V. One hour later the potential was stepped to the value of interest, e.g., +0.344 V, and cyclic voltammograms such as those in Fig. 3 were obtained as a function of time. We used a scan rate of 0.1 V/s, although higher temporal resolution could be obtained with a faster scan rate. The rate constant was evaluated by considering peak splitting, ΔE_p, of the voltammograms. The logarithm of the rate constant was found to decrease linearly with the logarithm of time giving a slope of –0.2 (Fig. 8). Similar results were obtained for a film grown at 25°C with the electrolyte open to the atmosphere.

Influence of temperature.— The effect of temperature on the redox kinetics for Ru(NH$_3$)$_6^{3+/2+}$ was investigated over a range of 35°C using the same electrodes as those used for the film growth study. Typically, the electrode was held at a given potential for ~20 h at 30°C to produce an oxide film of given thickness, d. Voltammograms were taken as the electrochemical cell was cooled to ~0°C and brought back to 30°C. Temperatures greater than 30°C (the temperature of film growth) were not examined since additional film growth occurs. The thermal cycle took approximately 1 h to complete. Rate constants were obtained from the ΔE_p values (Fig. 9). The precision of these measurements was not great due to a maximum variation in the peak splitting of ~10 mV over the temperature range investigated. This difference is the same order of magnitude as the normalization constant (temperature-dependent diffusion coefficient, etc., Eq. 1, 3) used to derive the rate constant k_{eff}^o from the dimensionless rate paramter Λ. Significant scatter is apparent among the three data sets with the activation energy ranging from a maximum of 0.15 to 0 eV. The solid line in Fig. 9 is the thermal dependence predicted by the model described in the Discussion section. The slope of this curve corresponds to an activation energy (0.15 eV), while the absolute magnitude of the curve was arbitrarily set for easy comparison with the experimental data.

Passive Film Thickness, Å
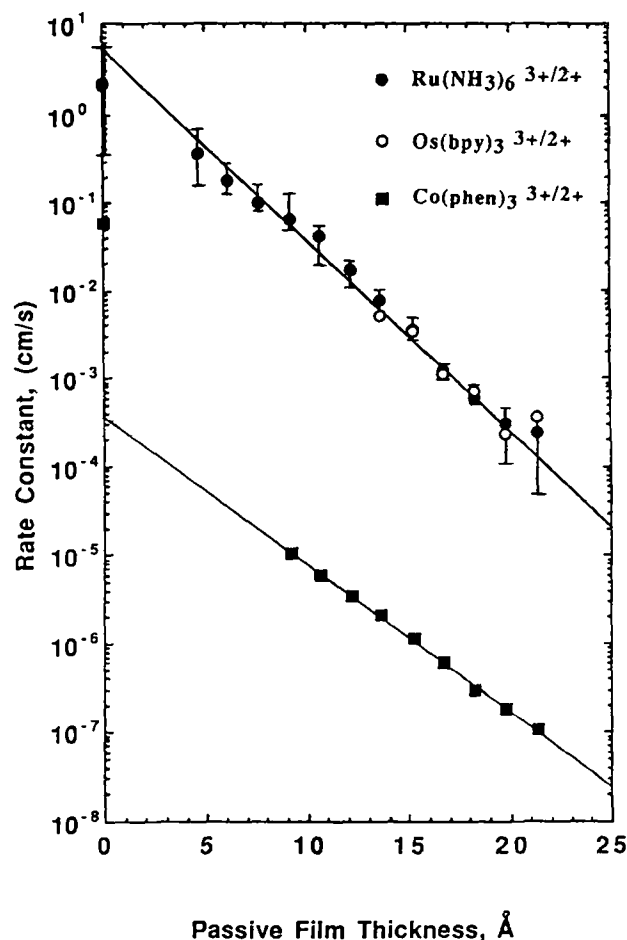
Fig. 7. The apparent rate constant as a function of passive-film thickness. The line through the Ru(NH$_3$)$_6^{3+/2+}$ data corresponds to β = 0.215 Å^{-1} while β = 0.164 Å^{-1} for the Co(phen)$_3^{3+/2+}$ data. The intrinsic rate constant on gold is indicated on the film-thickness axis, at $d = 0$.

Discussion

Qualitatively, the relationship between the rate constant and film thickness (Fig. 7) may be a consequence of electron tunneling through the thin dielectric passive film. However, if there is significant spatial variation in film thickness, the passivated electrode also can be treated as a partially blocked electrode. These two ideas will be developed below.

Electron tunneling.—In the case of elastic tunneling through a homogeneous barrier, the constant β (Eq. 6) defines the blocking character of the film.[5,6] To develop a quantitative description of β requires a physical model of the passive oxide interface. Figure 10 shows a schematic of the electronic structure of the interface. We used this schematic to generate a simple equation for the electrode kinetics based on the fluctuating energy model[6] that is analogous to the more sophisticated transfer Hamiltonian formalism developed by Schmickler and Ulstrup.[5] We assume that the effective oxide bandedges at the film/solution interface are fixed and determined by the solution pH via OH$^-$/H$^+$ equilibria. This is equivalent to the potential drop across the Helmholtz layer at the oxide/solution interface being independent of the potential of the passive electrode with respect to the reference electrode, *i.e.*, for the voltammetric experiments a potential change of the metal, with respect to the reference electrode, causes a change in the electric field only within the oxide film. Prior impedance[1,2] and polarization[14] measurements support this assertion and also demonstrate that the dielectric constant of the film is independent of thickness. Electron transfer proceeds by tunneling between occupied and unoccupied states of equal energy in the metal and the electrolyte. The probability of
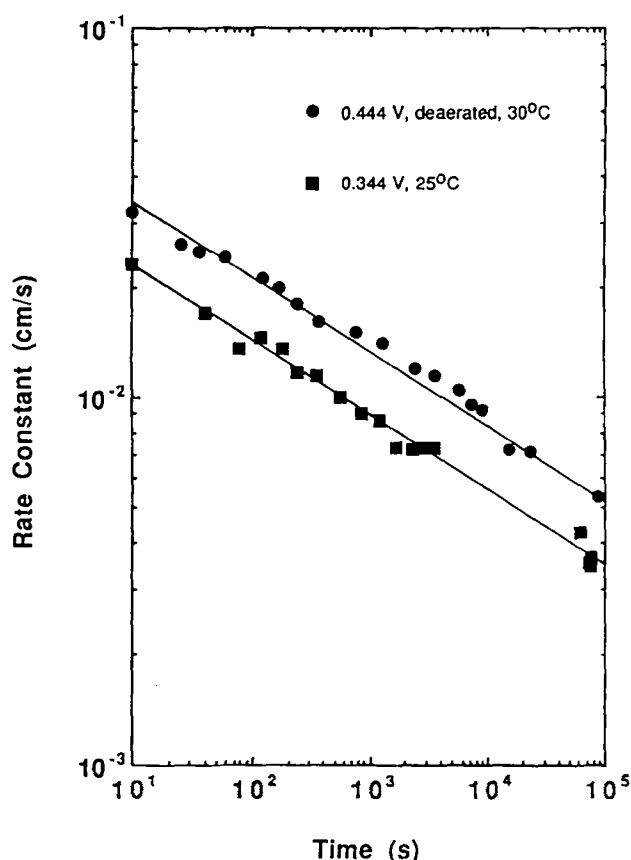
Fig. 8. The rate constant for Ru(NH$_3$)$_6^{3+}$ reduction measured as a function of time following a potential step from –0.156 V to the value indicated.

finding occupied states in the metal electrode is described by the Fermi-Dirac distribution function

$$F(\varepsilon, \eta) = \frac{1.0}{\exp\left(\frac{\varepsilon + e\eta}{kT}\right) + 1} \qquad [7]$$

where η is the overpotential (η = $E - E^{o'}$), *e* is the electronic charge, and ε is the electron energy in the metal relative to the Fermi level of the redox couple. In the electrolyte, the electronic states are localized at the reduced and oxidized species. The energy depends on the configuration of the reactive complex. Thermal fluctuations produce a Gaus-
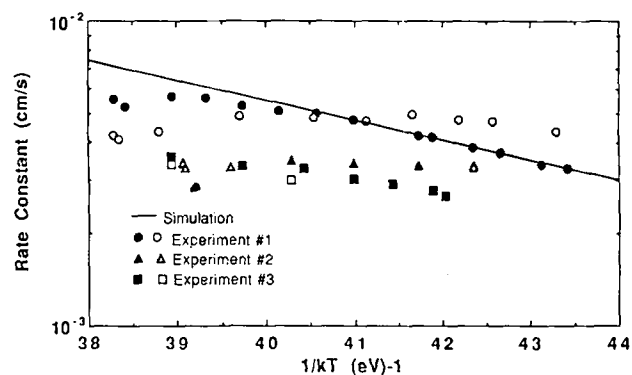
Fig. 9. The temperature dependence of the rate constant for Ru(NH$_3$)$_6^{3+/2+}$ after more than 20 h of potentiostatic polarization. The solid data points correspond to the cooling cycle, and the open points to the warming cycle. The solid line is a simulation based on the model given in the text. The activation energy is given by the slope of the curve (0.15 eV); however, the absolute magnitude was arbitrarily chosen for comparison with the experimental data. Conditions: Experiment #1, $E = 0.444$ V, deaerated with argon; Experiment #2, #3, $E = 0.344$ V, open to atmosphere.
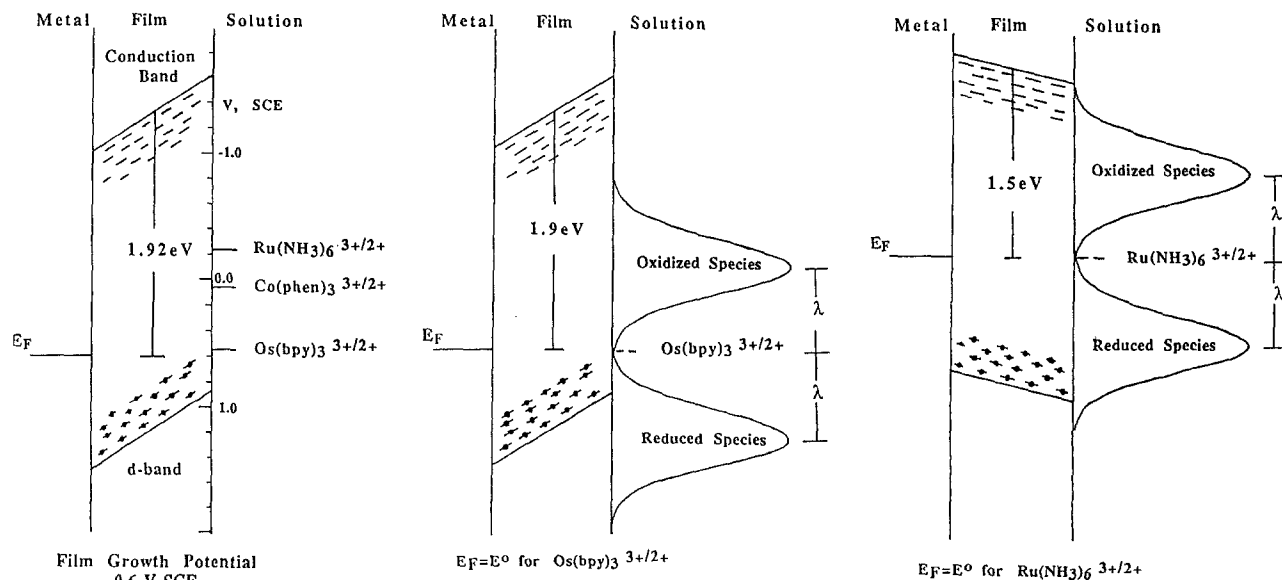
Fig. 10. A schematic of the electronic structure of the passive electrode for a film grown at 0.6 V.

sian distribution around the most probable state which is defined by the reorganization energy, λ.[6] Consequently the probability of finding an oxidized or reduced species on the saddle point of the reaction hypersurface is given by

$$D_{ox}(\varepsilon) = \frac{1}{(\pi k T \lambda)^{1/2}} \exp\left(\frac{-(\varepsilon - \lambda)^2}{4kT\lambda}\right) \qquad [8]$$

$$D_{red}(\varepsilon) = \frac{1}{(\pi k T \lambda)^{1/2}} \exp\left(\frac{-(\varepsilon + \lambda)^2}{4kT\lambda}\right) \qquad [9]$$

For $Ru(NH_3)_6^{3+/2+}$, the solvent reorganization energy for the bimolecular self-exchange reaction is 1.3 eV.[17] Therefore a value of 0.65 eV was used for each redox species. On a bare metal electrode, the tunnel factor, κ, is arbitrarily taken as unity, $\kappa^o = 1$. However, the presence of the passive film results in a decrease of this probability. The energy barrier assumes a trapezoidal shape due to the electric field within the oxide film.[6] Therefore the tunneling probability is given by

$$\kappa(\varepsilon,\eta) = \kappa^o \exp\left(-\frac{4\pi(2m_e)^{1/2}}{h} d(r_{eff}(\varepsilon_B - 0.5e\eta - \varepsilon))^{1/2}\right) \qquad [10]$$

where r_{eff} is the ratio of the effective mass of the tunneling electron to the free electron mass, m_e, and ε_B is the barrier height, in eV, at zero overpotential, $e\eta = 0$. If the reaction rate is not limited by diffusion of redox species to the interface, the rate can be calculated, since the cathodic current density, j, is proportional to the product of the density of occupied states in the metal, unoccupied states in the electrolyte, and the probability of electron tunneling across the oxide, and vice versa for the anodic current[6]

$$j(\eta) = \int [(1 - F(\varepsilon, \eta))(D_{red}(\varepsilon))(\kappa(\varepsilon, \eta))$$
$$- (F(\varepsilon, \eta))(D_{ox}(\varepsilon))(\kappa(\varepsilon, \eta))]d\varepsilon \qquad [11]$$

For our calculations the energy integral was evaluated between 3λ and -3λ in 0.001 eV increments. Tafel curves were generated by progressively stepping the overpotential from 0 to 0.5 V in 10 mV increments. A variety of film-thickness values, over a range of temperatures, was investigated for various barrier properties (r_{eff}, ε_B). Not surprisingly (Fig. 11) this model deals effectively with the logarithmic decrease of the rate constant with film thickness and the potential dependence of the transfer coefficient (Fig. 5, 6). Multiplying Eq. 11 (Fig. 11) by a pre-exponential collisional frequency term, typically 10^3 to 10^4,[6] gives a favorable comparison between the model and the absolute magnitude of the rate constant determined by experiment. The simulations also reveal that electron transfer becomes

asymmetric with increasing film thickness. These effects are in agreement with the theory presented by Schmickler and Ulstrup.[5] The asymmetry is a consequence of the energy distribution of the tunneling current. The tunneling probability decreases with an increase in the film thickness and barrier height. This results in electrons from above the Fermi level contributing significantly to the current. The experimentally determined β value does not yield a unique solution for ε_B and r_{eff}, rather it defines the possible combinations. However, close consideration of the model reveals additional constraints. The asymmetry of the transfer
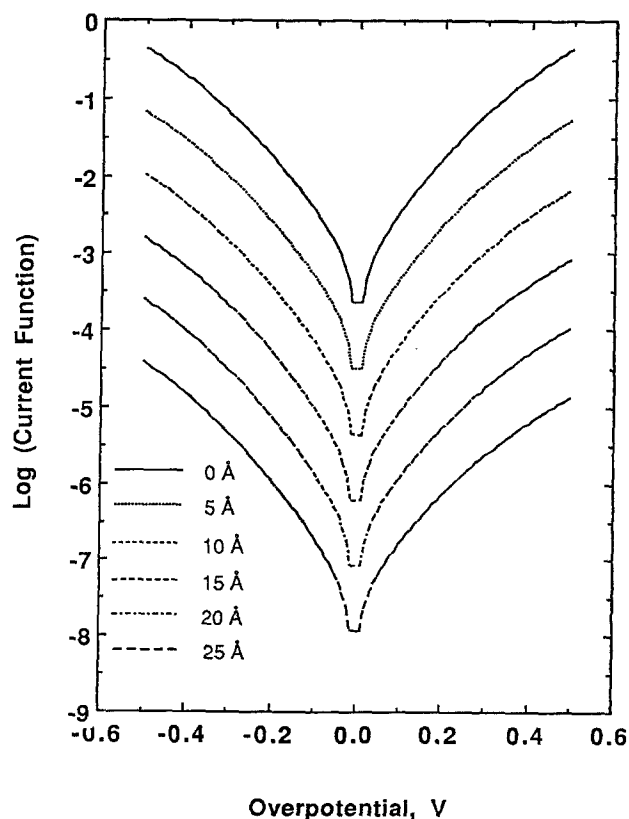
Fig. 11. An example of a Tafel plot calculation performed for a range of film thickness, for $\varepsilon_B = 1.5$ eV and $r_{eff} = 0.1$ using Eq. 11. Multiplication of the current function by a pre-exponential constant of 10^3 or 10^4 and examination of the rate at $\eta = 0$ yields a favorable comparison with the absolute value of the data given in Fig. 4.

coefficient is related to the magnitude of the barrier, and this is a function of the formal potential of the probing redox couple as revealed in Fig. 10.

While reliable independent measurements of either of these parameters are limited, photoelectrochemical studies[18] of the passive film on chromium indicate an optical gap ranging from 2.4 to 3.3 eV depending on the film-formation conditions. Both anodic and cathodic photocurrents were reported. In a similar vein, *in situ* modulated reflectance studies of the anodically formed film reveal two weak ligand-field transitions, at 3.1 and 4.9 eV, which were ascribed to chromic ions octahedrally coordinated to oxide species.[13] These results in combination with x-ray photoelectron (XPS) valence-band spectra and knowledge of the electric field within the film, $\sim 4 \times 10^6$ V/cm,[2] were used to define the semiquantitative description of passive chromium (Fig. 10). The XPS data suggest a difference of at least 1.0 eV between the metal Fermi level and the d-band states. The mobility gap was taken to be ~ 2.4 eV. The subgap "dash" and "dot" structures in Fig. 10 denote localized states which follow from defects or the lack of long-range order. Good agreement between the experimental results and the simulation required $r_{eff} = 0.1$ for the tunneling electrons. An example of the dependence of the calculated rate constant on film thickness is shown in Fig. 12.

The temperature dependence of the rate constant for this model also was examined. While the tunneling component is temperature independent, the density of redox states in solution is thermally populated with an activation energy of $\lambda/4$ or 0.16 eV. The simulation yields an activation energy of 0.15 eV for the passivated electrode, which is within the scatter of the experimental data (Fig. 9).

Partially blocked electrode.— An alternative theoretical approach to this problem is the partly blocked electrode treatment developed by Amatore *et al.*[19] This theory predicts a decrease in the apparent rate constant as a consequence of a corresponding decrease in the active electrode area

$$k_{eff}^0 = \theta k^0 \qquad [12]$$

where θ is the surface coverage of active unblocked area. According to this scheme, the experimental data for passivated chromium indicate that the active area decreases exponentially with increasing film thickness

$$\log(k_{eff}^0) = \log(k^0) + \log(\theta) = \log(\mathcal{A}) - \beta d \qquad [13]$$

In this instance β (Eq. 4) characterizes the relationship between the active electrode area and the average film thickness. In the original theory,[19] the active area is viewed as regions of bare unblocked metal. While congruence of the $Ru(NH_3)_6^{3+/2+}$ and $Os(bpy)_3^{3+/2+}$ data is consistent with this picture, the notion of film-free domains of chromium metal occurring at passive potentials is physically unintuitive. Nonetheless the passive-film thickness may vary about the mean value reported in Fig. 1. Prior oxidation studies[20] suggest that the film thickness is significantly dependent on crystallographic orientation and also may be a distributed parameter within a single grain. Thus, elements of both tunneling theory and the partly blocked electrode formalism must be combined to treat the data realistically.

Active sites of enhanced tunneling probability.— Conventional expressions for electron tunneling indicate that the probability of transfer is critically dependent upon the thickness of the insulating overlayer. Thus, variations in thickness result in a distribution of active sites of enhanced tunneling probability. The existence of such sites has been well documented in a recent study of the native oxide found on the silicon (100) surface.[21] Transmission electron microscopy analysis of a cross section of this interface revealed that the native oxide thickness ranged from 5 to 15 Å over small lateral distances ~ 80 Å. A complementary scanning tunneling microscopy investigation demonstrated that the thin active sites account for not more than 20% of the geometrical surface area. Similarly, for metal-insulator-metal tunnel junctions, agreement between theory and experiment typically requires specification of an active tunneling area corresponding to 1-30% of the geometrical area.[22] Such a scaling factor explains the discrepancy between the rate constant for $Co(phen)_3^{3+/2+}$ reduction on gold (determined by cyclic voltammetry, ΔE_p) and the value obtained by extrapolation of the chromium-passive film data (extracted from Tafel plots (Fig. 7).

The simple application of the active-area concept is tantamount to applying a scaling constant to the rate data. However consideration of the nature of the active site, a thin point of enhanced tunneling, demands a reevaluation of the film-thickness data used in Fig. 7. This problem has been treated theoretically by Chow[23] and Hurych.[24] A tunneling barrier was developed by building up a film through random deposition of atoms. Consequently, the Poisson distribution function was used to describe the variation in film thickness. The thickness, $d_{capacitance}$, derived from capacitance measurements was close to that of the mean value, $d_{average}$, of the distribution, while the effective tunneling distance, d_{tunnel}, was found to be equal to one half of that determined by capacitance, $d_{tunnel} \sim 0.5 d_{average}$. Good agreement was found between this model and experimental data for $Al-AlO_x-Al$ tunnel junctions. Thus a revised treatment of the passive interface would involve a tunneling process with appropriate corrections made for the active area and the corresponding film thickness at such sites. Further progress on this issue requires a more direct experimental assessment of the active surface regions. Studies by scanning electrochemical microscopy may provide an approach to this issue.[25]

Applications.— The strong dependence of the electron-transfer rate on the conditions of film formation suggest possible applications for the chromium electrode. Currently there is interest in modifying electrodes with Langmuir-Blodgett and self-assembling organic layers. These
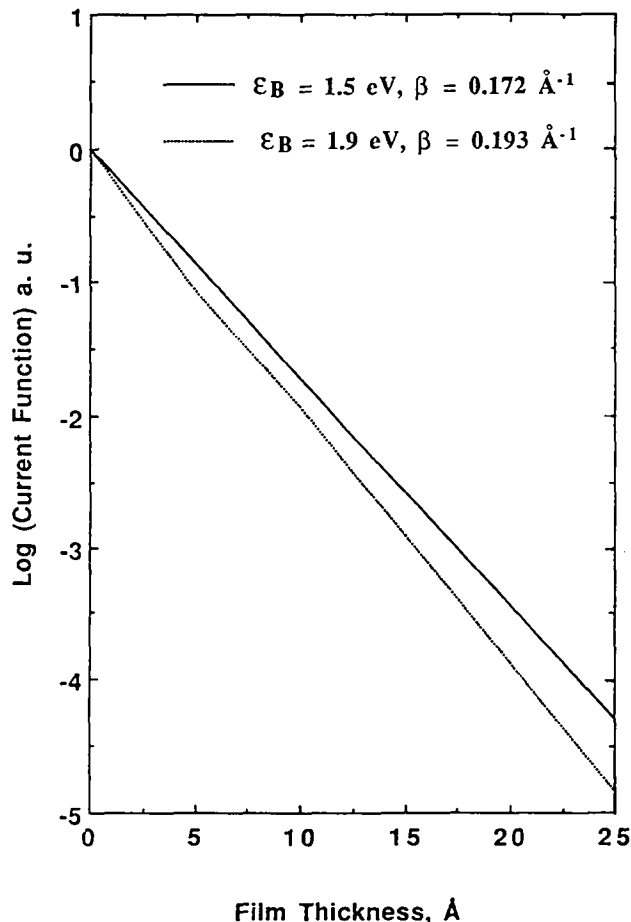
Fig. 12. A simulation of the influence of film thickness on the electron-transfer rate constant, at η = 0, for the barrier parameters specified in Fig. 10 and r_{eff} = 0.1.

films bring an array of unique interfacial properties to electrochemistry. For example, in a manner analogous to passive chromium, the rate of electron transfer across hydroxl-terminated alkylthiol layers on gold is a function of the length of the alkyl chain.[12] These structures have been proposed for examining high rate constants, as well as for probing the electronic state densities of solvated redox species.[12,26] Similarly, it is possible to impart novel characteristics to metal oxide surfaces by forming self-assembling monolayers (SAM) by adsorption of appropriate precursors.[27] The ability to form complex, addressable, chemical microstructures also has been demonstrated, *e.g.*, an array of alternating Au and Al/Al$_2$O$_3$ band electrodes with chemically distinct self-assembled organic overlayers.[28] The influence of the passive chromium oxide layer on electron-transfer kinetics for a similar interdigitated array of Au and Cr electrodes recently was demonstrated by scanning electrochemical microscopy.[29] Thus, careful pretreatment of the chromium electrode could provide an added degree of freedom in the design of metal/metal oxide/SAM interfaces for electrochemical applications (*i.e.*, give a rate constant for electron transfer which is a function of the passive-film thickness in series with the characteristics of the overlaying SAM).

Another possible extension of this study derives from interest in techniques for examining the passivity of metals. During the last fifteen years, significant advances in understanding have been driven by the development of UHV techniques, *e.g.*, x-ray photoelectron spectroscopy. However in many instances the *ex situ* nature of the UHV experiment perturbs the interface under study leading to artifacts which are difficult to resolve. Studies of the kinetics of electron transfer should provide a sensitive measure of such changes. Thus, redox measurements performed before and after the *ex situ* UHV experiment should yield an assessment of such changes.

Conclusion

The kinetics of electron transfer between electrochemically passivated chromium and several outer-sphere redox couples have been investigated as a function of passive film thickness, $d = 5$ to 25 Å. The thickness of the dielectric passive overlayer can be defined by using rigorously controlled film-formation conditions. The redox rate decreased exponentially with increasing thickness of the passivating film. Similarly, during potentiostatic film growth, the electron-transfer rate decreases logarithmically with time, and this is correlated with the film-growth kinetics, *i.e.*, d is proportional to log(t). These observations may be attributed to either a homogeneous tunneling barrier or a partly blocked electrode. However these formalisms are highly simplified, and the basic tenets of each model were violated. Nonetheless, a combination of these ideas can explain the experimental results qualitatively, although a meaningful quantitative treatment remains elusive until the precise microstructural nature of the film is defined clearly.

Acknowledgment

LIST OF SYMBOLS

	pre-exponential constant
A	electrode area
β	tunneling constant
C_o	concentration of redox species
d	thickness of passive film
D, $D(T)$	diffusion coefficient of redox species (temperature dependent)
D_{ox} (ε)	probability distribution of energy states in the oxidized species
D_{red} (ε)	probability distribution of energy states in the reduced species
ΔE_p	absolute difference between E_{pa} and E_{pc}
E	electrode potential
$E^{o'}$	formal potential
E_{pa}	potential of anodic voltammetric peak
E_{pc}	potential of cathodic voltammetric peak
$E_{pc/2}$	potential at half the cathodic peak current
ε	electronic energy
e	electric charge of electron
F	Faraday's constant
$F(\varepsilon, \eta)$	Fermi function; density of occupied states in the solid
h	Planck's constant
i_o	exchange current
$j(\eta)$	current density
k^o	rate constant for redox couple on an inert electrode, *i.e.*, Au
k^o_{eff}	rate constant for redox couple on passivated chromium
k	Boltzmann's constant
κ	tunneling probability
κ^o	pre-exponential factor for the tunneling probability
m_e	free electron mass
n	number of electrons or equivalents
r_{eff}	ratio of the effective mass to the free-electron mass, m_e
R	gas constant
T	temperature
α	transfer coefficient for a redox couple on an inert electrode
α_{eff}	transfer coefficient for a redox couple on passivated Cr
λ	reorganization energy of a redox couple
η	overpotential, $\eta = E - E^{o'}$
θ	surface coverage
v	scan rate
$\Psi(E)$	current function
Λ	dimensionless rate parameter

REFERENCES

1. H. Haupt and H. H. Strehblow, *J. Electroanal. Chem.*, **278**, 365 (1987); *ibid.*, **216**, 229 (1987).
2. T. P. Moffat and R. M. Latanision, *This Journal*, **139**, 1869 (1992); and references cited therein.
3. T. Heumann and F. W. Diekotter, *Ber. Bunsenges. Phys. Chem.*, **67**, 671 (1963).
4. A. M. Sukhotin, E. I. Antonovskaya, and A. A. Pozdeeva, *Russian J. of Phys. Chem.*, **36**, 11 (1962).
5. W. Schmickler and J. Ulstrup, *Chem. Phys.*, **19**, 217 (1977); W. Schmickler, *J. Electroanal. Chem.*, **84**, 203 (1977).
6. H. Gerischer, *Electrochim. Acta*, 1677 (1990); J. W. Schultze, *Passivity of Metals*, R. P. Frankenthal and J. Kruger, Editors, p. 82, The Electrochemical Society, Inc., Princeton, NJ (1978); W. Schmickler and J. W. Schultze, *Modern Aspects of Electrochemistry*, J. O'M Bockris, B. E. Conway, and R. E. White, Editors, Plenum Press, New York (1986); S. R. Morrision, *Electrochemistry at Semiconductor and Oxidized Metal Electrodes*, Plenum Press, New York (1980).
7. L. Y. L. Shen, *J. Appl. Phys.*, **40**, 5171 (1969); R. C. Jaklevic and J. Lambe, *Phys. Rev. B*, **2**, 808 (1970).
8. S. Kapusta and N. Hackerman, *This Journal*, **128**, 327 (1981).
9. M. Prazak and T. X. Sen, *Electrochim. Acta*, **21**, 509 (1976).
10. R. Memming and F. Mollers, *Ber. Bunsenges. Phys. Chem.*, **76**, 475 (1972).
11. J. W. Schultze and K. J. Vetter, *Electrochim. Acta*, **18**, 889 (1973).
12. T. T.-T. Li and M. J. Weaver, *J. Am. Chem. Soc.*, **106**, 6107 (1984); E. Sabatani and I. Rubinstein, *J. Phys. Chem.*, **91**, 6663 (1987); C. E. D. Chidsey, *Science*, **251**, 919 (1991); C. Miller, P. Cuendot, and M. Gratzel, *J. Phys. Chem.*, **95**, 877 (1991).
13. N. Hara and K. Sugimoto, *This Journal*, **126**, 1328 (1979).
14. K. Sugimoto and S. Matsuda, *Mater. Sci. and Eng.*, **42**, 181 (1980); M. A. Genshaw and R. S. Sirohi, *This Journal*, **118**, 558 (1971); R. Saito and N. Sato, *ibid.*, **127**, 1901 (1980).

15. T. Iwasita, W. Schmickler, and J. W. Schultze, *Ber. Bunsenges. Phys. Chem.*, **89**, 138 (1985).
16. (a) A. J. Bard and L. R. Faulkner, *Electrochemical Methods*, John Wiley & Sons, Inc., New York (1980); (b) H. Matsuda and Y. Ayabe, *Z. Elektrochem.*, **59**, 494 (1955).
17. R. A. Marcus and N. Sutin, *Biochim. Biophys. Acta*, **811**, 265 (1985).
18. C. Sunseri, S. Piazza, and F. DiQuarto, *This Journal*, **137**, 2411 (1990); N. Hara, A. Yamada, and K. Sugimoto, *J. Jpn. Inst. Metals*, **49**, 640 (1985).
19. C. Amatore, J. M. Saveant, and D. Tessier, *J. Electroanal. Chem.*, **146**, 37 (1983); **147**, 39 (1983).
20. J. S. Foord and R. M. Lambert, *Surf. Sci.*, **161**, 513 (1985).
21. A. H. Carim, M. M. Dovek, C. F. Quate, R. Sinclair, and C. Vorst, *Science*, **237**, 630 (1987).
22. J. G. Simmons, *Transactions of the Metallurgical Society of AIME*, **233**, 485 (1965).
23. C. K. Chow, *J. of Appl. Phys.*, **34**, 2599 (1963).
24. Z. Hurych, *Solid-State Electron.*, **9**, 967 (1966).
25. D. O. Wipf and A. J. Bard, *This Journal*, **138**, L4 (1991); A. J. Bard, F-R. F. Fan, D. T. Pierce, P. R. Unwin, D. O. Wipf, and Feimeng Zhou, *Science*, **254**, 68 (1991).
26. A. J. Bennett, *J. Electroanal. Chem.*, **60**, 125 (1975); H. Morisaki, H. Ono, and K. Yazawa, *This Journal*, **135**, 382 (1982); *ibid.*, **136**, 1710 (1989); *ibid.*, **137**, 2759 (1990); K. Kobayashi, Y. Aikawa, and M. Sukigara, *J. Electroanal. Chem.*, **134**, 11 (1982); *Bull. Chem. Soc. Jpn.*, **55**, 2820 (1982).
27. D. L. Allara and R. G. Nuzzo, *Langmuir*, **1**, 45 (1985); *ibid.*, **1**, 52 (1985).
28. P. E. Laibinis, J. J. Hickman, M. S. Wrighton, and G. M. Whitesides, *Science*, **245**, 845 (1989).
29. C. Lee and A. J. Bard, *Anal. Chem.*, **62**, 1906 (1990).

Corrosion Inhibition of Mild Steel by Cationic and Anionic Polymers in Cooling Water System

I. Sekine,* M. Sanbongi, H. Hagiuda, T. Oshibe, and M. Yuasa

Department of Industrial Chemistry, Faculty of Science and Technology, Science University of Tokyo, 2641, Yamazaki, Noda, Chiba 278, Japan

T. Imahama, Y. Shibata, and T. Wake

Japan Organo Company, Limited, Central Research Laboratories, 1-4-9, Kawagishi, Toda, Saitama 335, Japan

ABSTRACT

The behavior of corrosion inhibition of mild steel by various cationic and anionic polymers, that is, polyethyleneimine (PEI), its derivative (PEID), polyarylamine (PAAm) and polydicyanodiamide derivative (PDCDA) as cationic polymers and polymaleic acid derivative (PMAD), polyacrylic acid derivative (PAAD) and polyacrylic acid (PAA) as anionic polymers, was investigated by corrosion tests and physicochemical measurements. Testing was done in two pseudoconcentrated solutions with low (LC) and high (HC) concentrations of ionic species like Ca^{2+} and Cl^-. The cationic polymers lacked inhibition ability, while the anionic polymers had a more effective inhibition ability. The anionic polymers had a potential to act as corrosion inhibitors of an adsorption-type in LC solution and as both corrosion inhibitors and scale inhibitors of calcium carbonate ($CaCO_3$). In LC solution, the inhibition efficiency (η) value of anionic polymers was dependent on number-average molecular weight ($\overline{M}_n$), content of carboxylic group (—COOH), and concentration of —COOH. In particular, the anionic polymers as inhibitors had an effective range of $\overline{M}_n$ (10^3 order). In HC solution, the degree of corrosion of steel was influenced by concentrations of both anionic polymers and solution components such as Ca ion ($CaCO_3$); the anionic polymers were competitively adsorbed with Ca ion on the steel.

An approach to corrosion inhibitors in a cooling water system has been based on chromate. This approach has generally been considered the most effective, but for environmental safety it was dropped from use. The use of other inorganic inhibitors such as zinc, molybdate, nitrites, and inorganic phosphate in cooling water systems has been investigated and reported.[1-3] Recently, attempts to minimize the need for such inorganic inhibitors have been made by incorporating organic materials into them. The studies of (all-)organic inhibitors as polymers, phosphonates, and carboxylic acids have been developed in cooling water systems.[4-12] The mechanism of corrosion inhibition of mild steel by organic inhibitors as polymers in cooling water systems has not been investigated. In this paper, to obtain a novel organic inhibitor without pollution control in cooling water systems, the behavior of corrosion inhibition of steels by various cationic and anionic polymers, that is, polyethyleneimine (PEI), its derivative (PEID), polyarylamine (PAAm), and polydicyanodiamide derivative (PDCDA) as cationic polymers and polymaleic acid derivative (PMAD), polyacrylic acid derivative (PAAD), and polyacrylic acid (PAA) as anionic polymers, was systematically investigated by corrosion tests and physicochemical measurements.

* Electrochemical Society Active Member.

Experimental

*Materials.—Inhibitors.—*The inhibitors used were polyethyleneimine (PEI, Wako Pure Chemical Industries), its derivative (PEID, Diafloc), polyarylamine (PAAm, Nitto Boseki), and polydicyanodiamide derivative (PDCDA, Diafloc) as cationic polymers, and polymaleic acid derivatives (PMAD), polyacrylic acid derivative (PAAD) and polyacrylic acid (PAA) as anionic polymers as shown in Table I. The cationic polymers were commercially purchased, and the anionic polymers were synthesized as follows.

Maleic acid (HOOC—CH=CH—COOH, MA, Wako Pure Chemical Industries) was reacted with α-olefin compounds and 1,4-butadiene. The crude products were purified by reprecipitation and dialysis to give poly(maleic acid-co-α-olefin) and poly(maleic acid-co-1,4-butadiene) (polymaleic acid derivatives, α-olefin type; PMAD-1 and PMAD-2 and 1,4-butadiene type; PMAD-3). Acrylic acid (CH_2=CH—COOH, AA, Wako Pure Chemical Industries) was reacted with sodium styrene sulfonate (CH_2=CH—C_6H_4—SO_3Na, NaSS, Tosoh) in distilled water containing ammonium peroxo-disulfate (Wako Pure Chemical Industries) and sodium hydrogen sulfate ($NaHSO_3$, Wako Pure Chemical Industries) at 55 to 90°C for about 30 min in a nitrogen atmosphere. The crude product